

Exploring the mechanism of phase transitions between the hexagonal close-packed and the cuboidal structures

Andres Robles-Navarro,[†] Shaun Cooper,[‡] Odile R. Smits,[¶] and Peter Schwerdtfeger^{*,†}

[†]*Centre for Theoretical Chemistry and Physics, The New Zealand Institute for Advanced Study, Massey University Auckland, Private Bag 102904, 0745 Auckland, New Zealand*

[‡]*School of Mathematical and Computational Sciences, Massey University Auckland, Private Bag 102904, Auckland 0745, New Zealand*

[¶]*Centre for Theoretical Chemistry and Physics, The New Zealand Institute for Advanced Study, Massey University Auckland, Private Bag 102904, 0745 Auckland, New Zealand, and the School of Mathematics and Physics, University of Queensland, Brisbane QLD 4072, Australia*

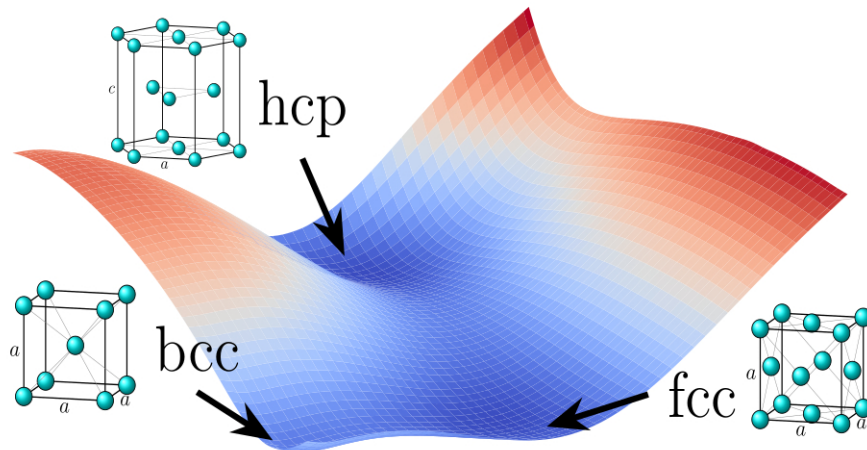
E-mail: peter.schwerdtfeger@gmail.com

Abstract

By introducing appropriate lattice parameters for a bi-lattice smoothly connecting the hexagonal close-packed (hcp) with the cuboidal structures, namely the body-centered (bcc) and the face centered cubic (fcc) lattices, we were able to map out the minimum energy path for a Burgers-Bain type of phase transition. We demonstrate that for three different models applied, i.e. the kissing hard-sphere model, the Lennard-Jones potential, and density functional theory for metallic lithium, the direct transition

path is always from hcp to fcc with a separate path leading from fcc to bcc. This solves, at least for the models considered here, a long-standing controversy of whether or not fcc acts as an intermediate phase in martensitic type of phase transitions.

TOC Graphic



Solid-state phase transitions are notoriously difficult to model.¹ While experimental methods can give quite detailed (P, T, V, μ, \dots) phase diagrams, the specific mechanism (dynamics) of a phase transition around the boundary line of different phases often eludes such experiments even for the simplest solids such as the rare gases. On the computational side, phase transition simulations are computationally very demanding and often plagued by the accuracy of the underlying model chosen for describing the intermolecular forces.^{2,3} Unlike in simple chemical reactions where the minimum energy path (MEP) from the reactants to the product can be obtained by certain algorithms⁴ and sophisticated electronic structure methods such as coupled-cluster theory,⁵ for the solid state it is often difficult to map out phase transition MEPs.⁶ Here one relies mostly on model potentials⁷ or on computationally demanding density functional theory and sophisticated algorithms like machine learning to explore the potential energy hypersurface.⁸⁻¹⁰

Martensitic transformations are a subclass of phase transitions described by diffusionless displacive transformations caused by lattice deformations where atoms move in a coordinated, homogeneous, and crystallographically oriented manner relative to their neighbors along some MEP.¹¹⁻¹³ It controls for example the mechanical properties of many materials such as steel at elevated temperatures.¹⁴ Bain described such a transition from fcc to bcc (the so-called Bain path) as early as in 1924 on purely crystallographic grounds,¹⁵ and Burgers later in 1934 in a similar fashion for the hcp to bcc transformation (Burgers path).¹⁶ While the former only involves changes in the basic lattice parameters a and $\gamma_2 = c/a$ within a cuboidal lattice, the latter is more complicated and involves a transition from a hexagonal based bi-lattice to some cuboidal (cub) lattices such as bcc.^{11,17} It remains, however, an open question whether there is a direct path from hcp to bcc or if the fcc lattice is an intermediate step in the Burgers hcp \rightarrow bcc transformation.¹⁸⁻²¹ For a recent discussion on lattice instabilities see Grimvall et al.¹¹

In order to map out the MEP between hcp and the cuboidal lattices, we developed

a simple and intuitive lattice model which we apply to three different models: the hard-sphere model,²² the (12,6)-Lennard-Jones potential,²³ and to metallic lithium using density functional theory.²⁴ Our treatment involves a much larger parameter space than previously applied²⁵⁻²⁷ and should therefore give a detailed insight into the combined Burgers-Bain type of phase transition.

We define the generator matrix $B = \{\vec{b}_1, \vec{b}_2, \vec{b}_3\}$ containing the lattice vectors \vec{b}_i and the shift vector \vec{v}_s as follows

$$B = a \begin{pmatrix} 1 & 0 & 0 \\ \frac{1}{2}\gamma_1(1 - \alpha) & \frac{1}{2}\gamma_1\sqrt{(1 + \alpha)(3 - \alpha)} & 0 \\ 0 & 0 & \gamma_2 \end{pmatrix}$$

$$\vec{v}_s^\top = \frac{a}{2}(\beta_1, \beta_2, \beta_3) \quad (1)$$

The B -matrix has been obtained from the conditions that (a) we have a linear transformation between the hexagonal and the cuboidal (cub) B -matrices defining the unit cell and characterized by the transformation parameter α , (b) we have a bi-lattice introducing a middle layer with the atom in the unit cell situated at the Wyckoff position \vec{v}_s as defined in eq.(1) and shown in Figure 1, (c) any distortion from the base lattice parameter $|\vec{b}_1| = |\vec{b}_2| = a$ is described by the lattice parameter γ_1 ($|\vec{b}_2| = \gamma_1 a$), and (d) we define $\gamma_2 = c/a$ as the ratio between the two lattice parameters in a Bravais lattice. We keep the angles between the vectors $\angle(\vec{b}_3, \vec{b}_1)$ and $\angle(\vec{b}_3, \vec{b}_2)$ at 90° reducing the problem from a complete 9 to a subset of 7 parameters for the lattices constants p_i , i.e. $\{p_i\} = \{\alpha, a, \gamma_1, \gamma_2, \beta_1, \beta_2, \beta_3\}$.

The transformation from bcc/fcc to hcp is visualized in Figure 1. The parameters for the three lattices are summarized in Table 1. From the table it is clear that the lattice parameter α is responsible for the hcp \rightarrow cub (cub = fcc or bcc) transformation through the angle θ_{12} between the vectors \vec{b}_1 and \vec{b}_2 , i.e. $\cos \theta_{12} = \frac{1}{2}(1 - \alpha)$, and the parameter γ_2 for the fcc \rightarrow bcc transformation.²⁸ This implies that we can describe the phase transition as a hypersurface

of the cohesive energy, $E_{\text{coh}}(\alpha, \gamma_2)$ with the remaining lattice parameters being optimized.

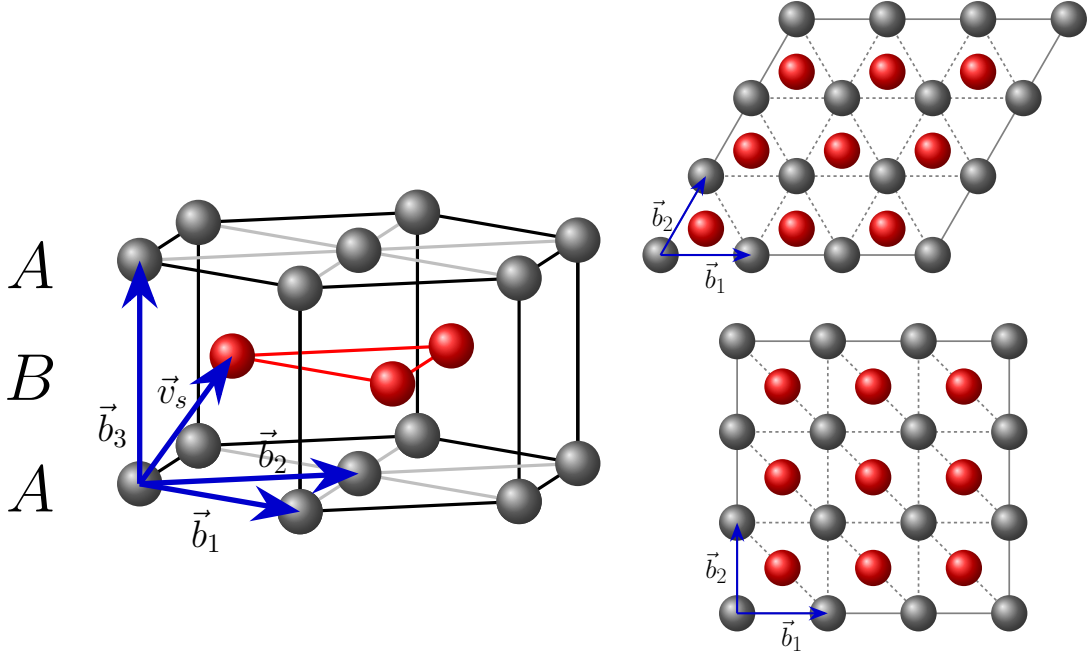


Figure 1: Left: The (distorted) cuboidal (blue lines shown on the left) and the hcp structure both with a ABABAB... sequence (layers A in red and B in blue) in a hexagonal unit cell with corresponding basis vectors. Right: The transformation between the cuboidal lattices fcc or bcc (top) and the hexagonal closed packed bi-lattice (bottom). The red atoms indicate the middle layer in the unit cell.

Table 1: Lattice parameters for kissing hard spheres of diameter 1 for the three lattices hcp, fcc and bcc. The volumes V , corresponding packing densities and kissing numbers N_{kiss} are also given.

Parameter	hcp	fcc	bcc
α	0	1	1
a	1	1	$\frac{2}{\sqrt{3}}$
γ_1	1	1	1
γ_2	$\sqrt{\frac{8}{3}}$	$\sqrt{2}$	1
β_1	1	1	1
β_2	$\frac{1}{\sqrt{3}}$	1	1
β_3	$\sqrt{\frac{8}{3}}$	$\sqrt{2}$	1
$\angle(\vec{b}_1, \vec{b}_2)$	60°	90°	90°
V	$\sqrt{2}$	$\sqrt{2}$	$\frac{8}{3\sqrt{3}}$
ρ	$\frac{\pi}{3\sqrt{2}}$	$\frac{\pi}{3\sqrt{2}}$	$\frac{\pi\sqrt{3}}{8}$
N_{kiss}	12	12	8

We can derive the volume of the unit cell using the B -matrix from (1)

$$V = \det(B) = \frac{a^3 \gamma_1 \gamma_2}{2} \sqrt{(1 + \alpha)(3 - \alpha)} \quad (2)$$

Since $V > 0$ we have the condition that $\alpha \in (-1, 3)$.

The kissing hard-sphere (KHS) model with attractive inverse power potential, called the Sutherland potential,²⁹ is defined by $\phi(r) = \infty$ for $r < 1$ and $\phi(r) = -r^{-n}$ for $r \geq 1$ (in reduced units). This model maximizes the number of nearest neighbors with distance 1, i.e. the kissing (or coordination) number N_{kiss} . For the cohesive energy we obtain $E_{\text{coh}} = -\frac{1}{2}L_{\frac{n}{2}}(p_i)$, where $L_{\frac{n}{2}}(p_i)$ are 3D infinite lattice sums dependent on the exponent n and the lattice parameters $\{p_i\}$ as defined in the generator matrix B . These are slowly converging sums which we treat efficiently to computer accuracy in terms of fast converging Bessel function expressions.³⁰ In the limit $n \rightarrow \infty$ we get $E_{\text{coh}} = -N_{\text{kiss}}/2$. The minimum energy conditions yields $a = 1, \gamma_1 = 1$ and $\beta_1 = 1$ for the hcp \rightarrow cub transition, leading to the expressions for the lattice parameters and the volume V derived from simple geometric arguments,

$$\gamma_2(\alpha) = \sqrt{\frac{8 + 4\alpha(1 - \alpha)}{4 - (1 - \alpha)^2}} \quad (3)$$

$$\beta_2(\alpha) = \sqrt{\frac{4 - (1 - \alpha)(\alpha + 3)}{4 - (1 - \alpha)^2}} \quad (4)$$

$$V(\alpha) = \sqrt{2 + \alpha(1 - \alpha)} \quad (5)$$

$\gamma_2(\alpha)$ is a monotonically decreasing function in the interval $\alpha \in [0, 1]$ changing from $\gamma_2(0) = \sqrt{\frac{8}{3}}$ to $\gamma_2(1) = \sqrt{2}$. Consequently, the KHS model directly connects the hcp with the fcc phase. The volume is at maximum at $\alpha = \frac{1}{2}$ with $V = \frac{3}{2}$, which we interpret as the transition state. Along the hcp \rightarrow fcc transition path the kissing number reduces to $N_{\text{kiss}} = 10$ for the

interval $\alpha \in (0, 1)$. For the r^{-6} attractive potential, for example, we locate the transition state at $\alpha^\# = 0.5000623690$ with an activation energy (with respect to the hcp structure) of $\Delta E_{\text{coh}}^\# = 0.7061966753$. The small deviation from the ideal $\alpha = \frac{1}{2}$ value comes from the fact that the hcp structure is slightly more stable compared to fcc by an energy difference of $\Delta E_{\text{coh}} = -4.881170486 \times 10^{-4}$.

If we proceed to the bcc phase the parameter γ_2 becomes now our reaction coordinate for the fcc→bcc Bain path. Here the 8 atoms at the edges of the cuboidal cell move slightly outwards as the unit cell gets compressed along the c -axis and we have $a > r_{\text{bc}} = 1$, where r_{bc} is the distance from the sphere at the origin of the unit cell to the one in the middle layer. The kissing number changes now from 12 (fcc) to 8 along the path to bcc. We can easily derive that

$$a(\gamma_2) = \frac{2}{\sqrt{2 + \gamma_2^2}} \quad \text{and} \quad V(\gamma_2) = \frac{8\gamma_2}{(2 + \gamma_2^2)^{\frac{3}{2}}} \quad (6)$$

In this case the volume is monotonically increasing from fcc to bcc. For the r^{-6} attractive potential, the bcc structure becomes a maximum at $\gamma_2 = 1.0$, with a difference to the fcc structure of $\Delta E_{\text{coh}} = 1.100126588$, which lies energetically even above the transition state for the hcp→fcc path. In this model the bcc phase is not stable towards distortion to the fcc structure.³¹

For a general (n, m) -LJ potential (in reduced units and $n > m$)²³

$$\phi_{\text{LJ}}(r) = \frac{nm}{n - m} \left[\frac{1}{nr^n} - \frac{1}{mr^m} \right] \quad (7)$$

we get the cohesive energy as a function of the lattice constant a for $m > 3$ to avoid divergencies³²

$$E_{\text{coh}}(p_i) = \frac{nm}{2(n - m)} \left[\frac{L_{\frac{n}{2}}(p_i)}{na^n} - \frac{L_{\frac{m}{2}}(p_i)}{ma^m} \right] \quad (8)$$

in terms of the lattice sums $L_{\frac{n}{2}}(p_i)$. As both lattice parameters connect the three phases hcp, fcc and bcc in a natural way, we map out the $E_{\text{coh}}(\alpha, \gamma_2)$ hypersurface to obtain a detailed insight into the phase transitions. To save computational time we restrict three of

the lattice parameters to their ideal values as shown in Table 1, i.e. $\gamma_1 = 1$, $\beta_3 = \gamma_2$ and $\beta_1 = 1$. Test calculations with a few random points in the parameter space revealed that the former two restrictions can be imposed and the latter is justified as it does not change the overall topology of the hypersurface. All other lattice parameters were optimized by using a Newton-Raphson procedure.³³

The $\Delta E_{\text{coh}}(\alpha, \gamma_2) = E_{\text{coh}}(0, \sqrt{\frac{8}{3}}) - E_{\text{coh}}(\alpha, \gamma_2)$ hypersurface for the (12-6)-LJ potential (taking the hcp structure as the reference) is shown in Figure 2. It is clear that there is no direct MEP from hcp to bcc; the MEP starting at hcp leads directly to the fcc structure as predicted from the simple KHS model. Further calculations reveal that neither of the more general (n, m) -LJ potentials have a direct MEP from hcp to bcc.³⁴ Starting from bcc towards the hcp structure, by changing the parameter α and optimizing all others, ends in steep ascend energetically. As discussed before,³¹ the bcc structure at $\alpha = 1$ and $\gamma_2 = 1$ is a maximum for the (12,6)-LJ potential. Concerning the transition state for the hcp→fcc path, we locate it at $\alpha^\# = 0.50036605$ with an activation energy of $\Delta E_{\text{coh}}^\# = 0.41488952$ relative to the hcp structure. The volume at the transition state is 1.32709616 and below the KHS limit as we expect for soft penetrating spheres.

For a real quantum system, we consider metallic lithium analyzed at the density functional theory (DFT) level. A detailed account of the lithium phase diagram has been given by Guillaume et al.³⁵ and Ackland et al.³⁶ Each point on the (α, γ_2) -energy hypersurface, as shown in Figure 2, corresponds to an optimization of a and β_2 at fixed values of α and γ_2 , together with $\gamma_1 = 1$, $\beta_1 = 1$ and $\beta_3 = \gamma_2$. The algorithm employed in the crystal structure optimization is the Newton-Raphson with the gradient and Hessian matrix calculated numerically through finite differences and ensuring an energy threshold for convergence of 10^{-6} eV in the electronic energy. The single-point calculations were performed with density functional theory using the Perdew-Burke-Ernzerhof (PBE) exchange-correlation functional³⁷ coupled to the dispersion corrections by means of the DFT-D3 approach including the Becke-Johnson damping function,^{38,39} as implemented in the VASP 6.4.0 version.^{40–44} The atomic cores are

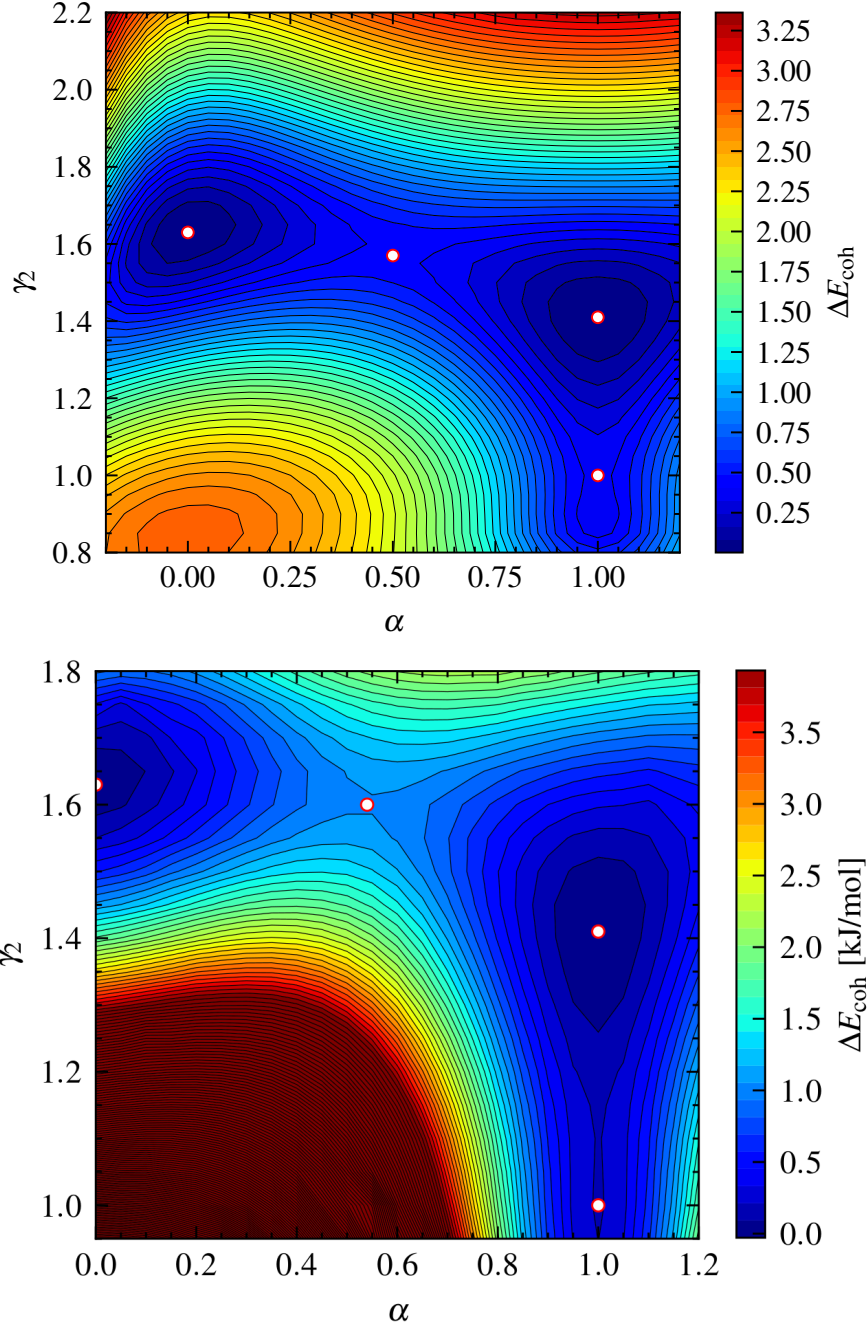


Figure 2: Cohesive energy hypersurface, $\Delta E_{\text{coh}}(\alpha, \gamma_2)$, with all other lattice parameters optimized for (top) the (12,6)-LJ potential (in reduced units), and (bottom) the lithium metal (in kJ/mol) calculated using the PBE-D3 functional. The white circles represent the position of the hcp ($\alpha = 0, \gamma_2 = \sqrt{8/3}$), hcp→fcc transition state ($\alpha \approx 0.54$), fcc ($\alpha = 1, \gamma_2 = \sqrt{2}$) and bcc ($\alpha = 1, \gamma_2 = 1$) structures.

described by the Projector Augmented Wave (PAW) method,⁴⁵ and the electronic minimization was done using the tetrahedron method⁴⁶ with Blöchl correction with an energy width

of 0.1 eV. The k -point grid was set using the keyword KSPACING=0.07 centered at the Γ point and an energy cut-off of 500 eV. The cohesive energies are obtained by comparing the energy of the bulk and the isolated atom, the latter calculated from a large orthorhombic unit cell of $14 \times 14.001 \times 14.002$ Å. Scanning the hypersurface and optimizing the lattice parameters is computationally very demanding.

Table 2: Lattice parameters and volume V for the hcp, fcc and bcc structures of lithium together with the transition states along the Burgers-Bain transformation path. The transition state of the hcp \leftrightarrow fcc transformation is denoted as TS₁, whereas for the fcc \leftrightarrow bcc is denoted by TS₂.

Prop.	hcp	fcc	bcc	TS ₁	TS ₂
E_{coh}	172.2216	172.2515	172.0344	171.1907	172.0212
α	0.000	1.000	1.000	0.541	1.000
a	2.962	2.963	3.325	2.9079	3.230
γ_2	1.632	1.411	1.000	1.599	1.095
β_2	0.577	1.000	1.000	0.820	1.000
V	36.731	36.708	36.757	38.268	36.900

Figure 2 shows that the topology of the lithium cohesive energy surface is quite similar to the one obtained for the (12, 6)-LJ potential, with the deepest minima located at the hcp and the fcc structures, fcc being the ground state, see Table 2. This is in agreement with a detailed phase diagram study of Ackland et al.³⁶ At standard conditions, the lithium metal is found in the bcc structure with a measured cohesive energy of 158 kJ/mol.⁴⁷ The difference from the experimental cohesive energy comes from temperature effects, zero-point vibrational contributions (3.971 kJ/mol for the fcc structure using the PBE functional⁴⁸) and the density functional approximation applied. We expect that this error is mostly compensated when taking energy differences along the transformation path.⁴⁸ The bcc structure of lithium is shown to be a very shallow minimum, in agreement with previous work.^{48,49} The path connecting hcp to the cuboidal structures leads directly to the fcc structure and has a transition state at $\alpha^\# = 0.541$ with an energy difference from hcp of $\Delta E_{\text{coh}}^\# = 1.031$ kJ/mol. The transformation from fcc to bcc occurs through a second transition state at $\gamma_2 = 1.095$

with an energy difference of $\Delta E_{\text{coh}}^{\#} = 0.230$ kJ/mol from the fcc phase. Noticeably, the hcp→fcc transition state lies energetically above the fcc→bcc Bain path. The maximum volume increase for the hcp→fcc transition is 4.18% compared to the hcp structure (see Table 2), and is less compared to the hard-sphere limit of 6.07% ($3/2\sqrt{2}$) as we expect.

In summary, for the unit cell, lattice parameters and three different interaction models applied we do not observe a direct minimum energy path from hcp to bcc as originally suggested by Burgers¹⁶ and others.^{26,27} The transition states on the (α, γ_2) -hypersurface MEP for lithium comes at rather low energies of about 1 kJ/mol. Classical molecular dynamics simulations at higher temperatures will explore the whole region of the parameter space outside the MEP,⁵⁰ and from such simulations it is therefore often difficult to get a detailed picture of the phase transition compared to directly mapping out the MEP as presented here. For solid-state systems such as barium,²⁸ or iron,⁵¹ where the bcc phase is significantly stabilized over the fcc or hcp phase,¹¹ the topology of the hypersurface is expected to change, which is the subject of our future investigations.

Acknowledgments

PS is grateful to Prof. Paul Indelicato (Kastler lab, Paris) for a visiting professorship at Sorbonne.

References

- (1) Liu, Xueyan,; Li, Hongwei,; Zhan, Mei, A review on the modeling and simulations of solid-state diffusional phase transformations in metals and alloys. *Manufacturing Rev.* **2018**, *5*, 10.

- (2) Hansen, J.-P.; Verlet, L. Phase Transitions of the Lennard-Jones System. *Phys. Rev.* **1969**, *184*, 151–161.
- (3) Chang, Y.; Chen, S.; Zhang, F.; Yan, X.; Xie, F.; Schmid-Fetzer, R.; Oates, W. Phase diagram calculation: past, present and future. *Prog. Mat. Sci.* **2004**, *49*, 313–345.
- (4) Schlegel, H. B. Exploring potential energy surfaces for chemical reactions: An overview of some practical methods. *J. Comput. Chem.* **2003**, *24*, 1514–1527.
- (5) Bartlett, R. J.; Musiał, M. Coupled-cluster theory in quantum chemistry. *Rev. Mod. Phys.* **2007**, *79*, 291–352.
- (6) Caspersen, K. J.; Carter, E. A. Finding transition states for crystalline solid–solid phase transformations. *Proc. Nat. Acad. Sci.* **2005**, *102*, 6738–6743.
- (7) Travesset, A. Phase diagram of power law and Lennard-Jones systems: Crystal phases. *J. Chem. Phys.* **2014**, *141*, 164501.
- (8) de Wijs, G. A.; Kresse, G.; Gillan, M. J. First-order phase transitions by first-principles free-energy calculations: The melting of Al. *Phys. Rev. B* **1998**, *57*, 8223–8234.
- (9) Jinnouchi, R.; Lahnsteiner, J.; Karsai, F.; Kresse, G.; Bokdam, M. Phase Transitions of Hybrid Perovskites Simulated by Machine-Learning Force Fields Trained on the Fly with Bayesian Inference. *Phys. Rev. Lett.* **2019**, *122*, 225701.
- (10) Liu, P.; Verdi, C.; Karsai, F.; Kresse, G. α – β phase transition of zirconium predicted by on-the-fly machine-learned force field. *Phys. Rev. Mater.* **2021**, *5*, 053804.
- (11) Grimvall, G.; Magyari-Köpe, B.; Ozoliņš, V.; Persson, K. A. Lattice instabilities in metallic elements. *Rev. Mod. Phys.* **2012**, *84*, 945–986.
- (12) Nishiyama, Z. *Martensitic transformation*; Elsevier, Amsterdam, 2012.

- (13) Lobodyuk, V.; Estrin, E. *Martensitic Transformations*; Cambridge International Science Publishing, 2014.
- (14) Venables, J. A. The martensite transformation in stainless steel. *Phil. Mag.* **1962**, *7*, 35–44.
- (15) Bain, E. The Nature of Martensite. *Trans. Am. Inst. Min. Metall. Eng.* **1924**, *70*, 25–46.
- (16) Burgers, W. On the process of transition of the cubic-body-centered modification into the hexagonal-close-packed modification of zirconium. *Physica* **1934**, *1*, 561–586.
- (17) Cayron, C. Continuous atomic displacements and lattice distortion during fcc–bcc martensitic transformation. *Acta Mat.* **2015**, *96*, 189–202.
- (18) Olson, G. B.; Cohen, M. A general mechanism of martensitic nucleation: Part I. General concepts and the fcc \rightarrow hcp transformation. *Metal. Trans. A* **1976**, *7*, 1897–1904.
- (19) Bruinsma, R.; Zangwill, A. Theory of the hcp-fcc transition in metals. *Phys. Rev. Lett.* **1985**, *55*, 214–217.
- (20) Akahama, Y.; Nishimura, M.; Kinoshita, K.; Kawamura, H.; Ohishi, Y. Evidence of a fcc-hcp Transition in Aluminum at Multimegabar Pressure. *Phys. Rev. Lett.* **2006**, *96*, 045505.
- (21) Lu, Z.; Zhu, W.; Lu, T.; Wang, W. Does the fcc phase exist in the Fe bcc–hcp transition? A conclusion from first-principles studies. *Model. Simul. Mater. Sci. Eng.* **2014**, *22*, 025007.
- (22) Baxter, R. J. Percus–Yevick Equation for Hard Spheres with Surface Adhesion. *J. Chem. Phys.* **1968**, *49*, 2770–2774.
- (23) Schwerdtfeger, P.; Wales, D. J. 100 Years of the Lennard-Jones Potential. *J. Chem. Theory Comput.* **2024**, *20*, 3379–3405.

- (24) Gross, E. K.; Dreizler, R. M. *Density functional theory*; Springer Science & Business Media, 2013; Vol. 337.
- (25) Straub, G. K.; Wallace, D. C. Study of the Martensitic Phase Transition in Sodium. *Phys. Rev. B* **1971**, *3*, 1234–1239.
- (26) Li, W.; Wang, T. Theoretical investigation of epitaxial deformation and the hcp-bcc transition of alkali metals. *Phys. Rev. B* **1999**, *60*, 11954–11962.
- (27) Raju Natarajan, A.; Van der Ven, A. Toward an Understanding of Deformation Mechanisms in Metallic Lithium and Sodium from First-Principles. *Chem. Mater.* **2019**, *31*, 8222–8229.
- (28) Chen, Y.; Ho, K. M.; Harmon, B. N. First-principles study of the pressure-induced bcc-hcp transition in Ba. *Phys. Rev. B* **1988**, *37*, 283–288.
- (29) Sutherland, W. LII. The viscosity of gases and molecular force. *London Edinburgh Philos. Mag. & J. Sci.* **1893**, *36*, 507–531.
- (30) Burrows, A.; Cooper, S.; Pahl, E.; Schwerdtfeger, P. Analytical methods for fast converging lattice sums for cubic and hexagonal close-packed structures. *J. Math. Phys.* **2020**, *61*, 123503.
- (31) Burrows, A.; Cooper, S.; Schwerdtfeger, P. Instability of the body-centered cubic lattice within the sticky hard sphere and Lennard-Jones model obtained from exact lattice summations. *Phys. Rev. E* **2021**, *104*, 035306.
- (32) Schwerdtfeger, P.; Gaston, N.; Krawczyk, R. P.; Tonner, R.; Moyano, G. E. Extension of the Lennard-Jones potential: Theoretical investigations into rare-gas clusters and crystal lattices of He, Ne, Ar, and Kr using many-body interaction expansions. *Phys. Rev. B* **2006**, *73*, 064112.

- (33) Hämmerlin, G.; Hoffmann, K.-H. *Numerical mathematics*; Springer Science & Business Media, Berlin, 2012.
- (34) Schwerdtfeger, P.; Cooper, S.; Smits, O.; Robles-Navarro, A. Connecting the hexagonal closed packed structure with the cuboidal lattices: A Burgers-Bain type martensitic transformation for a Lennard-Jones solid derived from exact lattice summations. 2024; <https://arxiv.org/abs/2406.09635>.
- (35) Guillaume, C. L.; Gregoryanz, E.; Degtyareva, O.; McMahon, M. I.; Hanfland, M.; Evans, S.; Guthrie, M.; Sinogeikin, S. V.; Mao, H.-K. Cold melting and solid structures of dense lithium. *Nature Physics* **2011**, *7*, 211–214.
- (36) Ackland, G. J.; Dunuwille, M.; Martinez-Canales, M.; Loa, I.; Zhang, R.; Sinogeikin, S.; Cai, W.; Deemyad, S. Quantum and isotope effects in lithium metal. *Science* **2017**, *356*, 1254–1259.
- (37) Perdew, J. P.; Burke, K.; Ernzerhof, M. Generalized Gradient Approximation Made Simple. *Phys. Rev. Lett.* **1996**, *77*, 3865–3868.
- (38) Grimme, S.; Antony, J.; Ehrlich, S.; Krieg, H. A consistent and accurate ab initio parametrization of density functional dispersion correction (DFT-D) for the 94 elements H-Pu. *J. Chem. Phys.* **2010**, *132*, 154104.
- (39) Grimme, S.; Ehrlich, S.; Goerigk, L. Effect of the damping function in dispersion corrected density functional theory. *J. Comput. Chem.* **2011**, *32*, 1456–1465.
- (40) Kresse, G.; Hafner, J. Ab initio molecular dynamics for liquid metals. *Phys. Rev. B* **1993**, *47*, 558–561.
- (41) Kresse, G.; Hafner, J. Ab initio molecular-dynamics simulation of the liquid-metal–amorphous-semiconductor transition in germanium. *Phys. Rev. B* **1994**, *49*, 14251–14269.

- (42) Kresse, G.; Furthmüller, J. Efficiency of ab-initio total energy calculations for metals and semiconductors using a plane-wave basis set. *Comput. Mat. Sci.* **1996**, *6*, 15–50.
- (43) Kresse, G.; Furthmüller, J. Efficient iterative schemes for ab initio total-energy calculations using a plane-wave basis set. *Phys. Rev. B* **1996**, *54*, 11169–11186.
- (44) Kresse, G.; Joubert, D. From ultrasoft pseudopotentials to the projector augmented-wave method. *Phys. Rev. B* **1999**, *59*, 1758–1775.
- (45) Blöchl, P. E. Projector augmented-wave method. *Phys. Rev. B* **1994**, *50*, 17953–17979.
- (46) Blöchl, P. E.; Jepsen, O.; Andersen, O. K. Improved tetrahedron method for Brillouin-zone integrations. *Phys. Rev. B* **1994**, *49*, 16223–16233.
- (47) Kittel, C. *Introduction to Solid State Physics*; John Wiley & Sons, Inc.: New York, 2004.
- (48) Robles-Navarro, A.; Jerabek, P.; Schwerdtfeger, P. Tipping the Balance Between the bcc and fcc Phase Within the Alkali and Coinage Metal Groups. *Angew. Chem. Int. Ed.* **2024**, *63*, e202313679.
- (49) Jerabek, P.; Burrows, A.; Schwerdtfeger, P. Solving a problem with a single parameter: a smooth bcc to fcc phase transition for metallic lithium. *Chem. Commun.* **2022**, *58*, 13369–13372.
- (50) Li, B.; Qian, G.; Oganov, A. R.; Boulfelfel, S. E.; Faller, R. Mechanism of the fcc-to-hcp phase transformation in solid Ar. *J. Chem. Phys.* **2017**, *146*, 214502.
- (51) Ekman, M.; Sadigh, B.; Einarsdotter, K.; Blaha, P. Ab initio study of the martensitic bcc-hcp transformation in iron. *Phys. Rev. B* **1998**, *58*, 5296–5304.